Hemodynamic Alterations in Portal Hypertension: A CFD-Based Study with Emphasis on Helical Flow Characteristics

Haonan Li¹, Zhenmin Fan^{1*}, Na Zhao¹, Xiaoyan Deng¹, Zhixiang Zhang^{2*}

¹School of Mechanical Engineering, Jiangsu University of Technology, Changzhou Jiangsu, China ²Department of Neurology, The Second People's Hospital of Changzhou, the Third Affiliated Hospital of Nanjing Medical University, Changzhou Medical Center of Nanjing Medical Universit. Changzhou, China

*Corresponding author: Zhenmin Fan, School of Mechanical Engineering, Jiangsu University of Technology, Changzhou Jiangsu, China, e-mail address: fanzhenmin2009@163.com; Zhixiang Zhang, Department of Neurology, The Second People's Hospital of Changzhou, the Third Affiliated Hospital of Nanjing Medical University, Changzhou Medical Center of Nanjing Medical Universit. Changzhou, China, e-mail address: zhixiangzhang@njmu.edu.cn

Submitted: 27th July 2025 Accepted: 25th October 2025

Abstract

Purpose: Portal hypertension (PHT) leads to complications such as variceal bleeding, hepatic remodeling, and thrombosis, driven by altered hemodynamics. This study aims to elucidate flow structure, shear stress, and helicity changes under PHT, and their potential roles in promoting thrombosis and vascular remodeling.

Methods: A patient-specific portal venous system model was reconstructed from CT images. Computational fluid dynamics (CFD) simulations were conducted to evaluate flow velocity, wall shear stress (WSS), oscillatory shear index (OSI), relative residence time (RRT), and helicity.

Results: Compared to the healthy model, the PHT condition demonstrated reduced flow velocity, lower TAWSS, and elevated RRT, particularly near bifurcations. Moreover, the strength and symmetry of helical flow were significantly impaired in PHT, especially at the main portal vein bifurcation—an area frequently associated with thrombosis.

Conclusions: This study highlights the role of hemodynamic disruption, particularly helicity loss, in the pathogenesis of PHT-related complications. CFD-based helicity analysis offers novel insight into biomechanical risk assessment and may inform future interventional strategies.

Keywords: Portal hypertension, CFD, Helicity, Wall shear stress, Portal vein thrombosis.

1 Introduction

Portal hypertension (PHT)—clinically significant when the hepatic venous pressure gradient (HVPG) ≥ 10 mmHg — arises when intra-hepatic microvascular distortion, fibrotic nodular compression, and/or organic stenosis of the portal vein (PV) trunk and its branches markedly elevate vascular resistance [5], [15], [19]. The ensuing pressure overload forces portal blood to bypass the liver via collateral channels at the distal esophagus, gastric fundus, rectum, and umbilical region, producing dilated varices whose rupture precipitates massive upper-gastrointestinal hemorrhage, hypovolemic shock, multi-organ failure, and a case-fatality rate approaching 10-20% [4]. In addition, PHT is tightly coupled to portal-vein thrombosis (PVT): sluggish flow, aberrant wall shear stress, and endothelial injury within the high-pressure milieu synergistically promote thrombus formation, further obstructing the PV and perpetuating a vicious hemodynamic cycle [16],[24]. A third and frequently overlooked consequence of sustained PHT is lobar volume remodeling. Extensive imaging and autopsy series have demonstrated progressive right-lobe atrophy with compensatory left-lobe hypertrophy in advanced cirrhosis [11]. This asymmetric growth is thought to reflect hemodynamic redistribution of splenic-vein (SV) and superior-mesenteric-vein (SMV) inflow within the PV: fibrous septa and regenerative nodules alter intrahepatic flow paths, channeling SV blood—rich in hepatotropic factors such as insulin and glucagon—preferentially toward the left lobe, while depriving the right lobe of adequate perfusion, oxygen, and nutrients. Collectively, these complex clinical sequelae underscore the pivotal yet incompletely elucidated role of portal hemodynamics in the pathogenesis of PHT-related complications.

Hemodynamic perturbations are now recognized as pivotal triggers of vascular wall remodeling and thrombogenesis. Across the spectrum from atherosclerosis to venous thrombo-embolism, experimental and clinical studies consistently demonstrate that adverse flow patterns—disturbed, recirculation zones, vortex shedding and flow separation—co-localize with low wall-shear stress (WSS), high oscillatory shear index (OSI) and relative residence time (RRT) [9],[26]. These mechanical cues are sensed by integrins, ion channels and the endothelial glycocalyx, activating

downstream some pathways that switch the endothelium from an anti-inflammatory, anti-thrombotic phenotype to a pro-inflammatory, pro-coagulant, and pro-proliferative state, increased release of von-Willebrand factor and tissue factor, and attenuation of eNOS [3],[13],[29]. Conversely, physiologic laminar flow—characterized by orderly streamlines and stable shear—maintains endothelial quiescence [1]. Beyond laminar flow, accumulating evidence highlights the protective role of coherent helical flow, commonly observed in the aorta, carotid bifurcation and other curved or branching arteries. Such helicity superimposes an axial-rotational velocity component that sustains favorable WSS levels, minimizes flow stagnation, and exhibits an even stronger "washing" effect that suppresses platelet deposition and inflammatory signaling [10],[25].

The hemodynamics of the portal venous system (PVS) are inherently complex, and perturbations become pronounced in PHT. Using vascular corrosion casting and scanning electron microscopy, C Van Steenkiste et al. [21] demonstrated marked microvascular alterations in mice with PHT and normal group exhibiting the highest WSS heterogeneity relative to sham and cirrhotic cohorts. Despite these observations, it remains unclear how such hemodynamic disturbances—particularly the presence or absence of helical flow—modulate the risk of PVT and lobar volume remodeling in cirrhotic patients with PHT.

Direct in-vivo quantification of portal hemodynamics and their pathological consequences remain technically challenging. CFD offers a powerful, non-invasive alternative. Qiu et al. [18] modeled the liver as a patient-specific porous medium to estimate portal-pressure gradients. Petkova et al. [14] showed, in an idealized geometry, that an intraluminal thrombus markedly distorts local velocity and shear fields. Liang et al. [23] linked splenectomy-induced geometric changes to prothrombotic flow patterns, while Zheng et al. [27] demonstrated that the SMV-SV confluence angle strongly modulates portal flow and thrombosis risk. These studies highlight CFD's value, yet a comprehensive analysis integrating helicity, shear metrics, while the potential influence of helicity on PHT-related complications is scarcely addressed.

Accordingly, we based on the CT-based, patient-specific 3D PVS model, Doppler velocities, and quantified the spatiotemporal distributions of four key metrics—time-averaged wall shear stress (TAWSS), OSI, RRT and helicity—across the reconstructed geometries. These CFD data are used to elucidate the relationship between aberrant flow patterns and their mechanical consequences on portal-vein thrombosis formation and lobar remodeling, providing quantitative evidence of how altered hemodynamic environments may contribute to pathological vascular changes.

2 Method

2.1. The computational models

The study was conducted in accordance with the Declaration of Helsinki and was approved by the Ethics Committee of the Second People's Hospital of Changzhou (No. 2022KY120-01). The participant received detailed information about the study and gave written informed consent prior to enrolment.

Figure 1 illustrates the complete reconstruction workflow. Computed tomography angiography (CTA) data were obtained from a 65-year-old healthy female using a multi-detector scanner, covering the thoracic to upper-abdominal region (Figure 1, step 1). The scan generated 817 axial slices (slice thickness = 0.625 mm; in-plane resolution = 512×512 pixels). Luminal contours of the portal-venous tree were manually segmented in Mimics (Materialise, Belgium) and the resulting surface mesh was smoothed in Geomagic Studio (3D Systems, USA) (Figure 1, step 2). The geometry comprises a main portal vein (length ≈ 67 mm, diameter ≈ 11 mm); right and left portal branches (lengths 53 mm and 33 mm, diameters 12 mm and 10 mm, respectively); and splenic, superior mesenteric and inferior mesenteric

veins measuring 109 mm, 42 mm and 42 mm in length (Figure 2(a)). All three inlets were extended—by 100 mm for the SV and at least 50 mm for the SMV and IMV—to ensure fully developed flow before entering the main computational domain (Figure 2b).

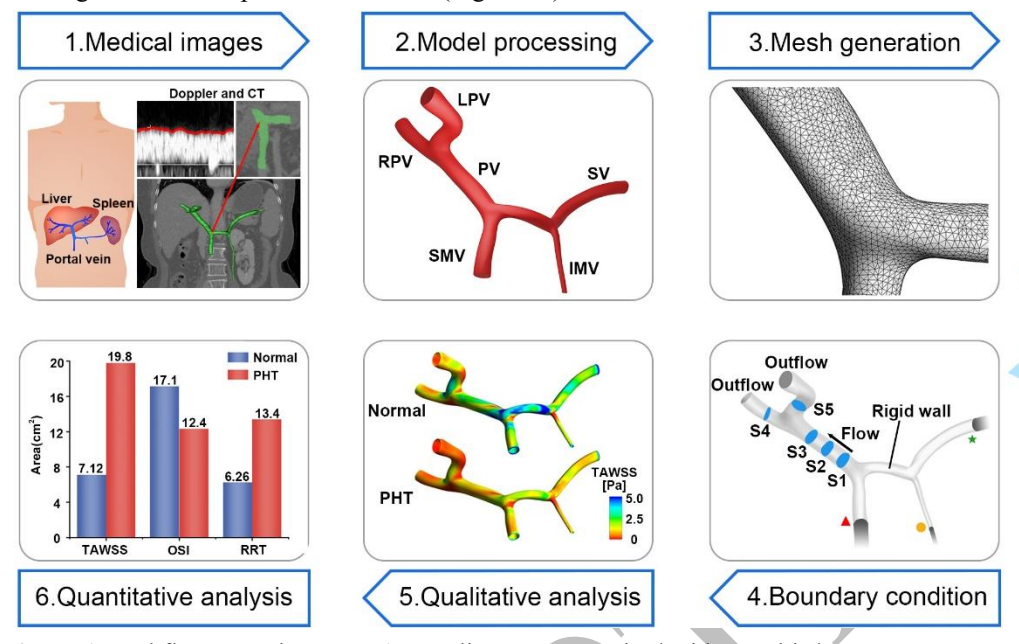


Figure 1 Workflow overview. Step 1: CT slices were acquired with a multi-detector scanner and used to reconstruct the three-dimensional portal-venous geometry. Step 2: The raw surface was smoothed and repaired. Step 3: A CFD mesh was generated with boundary-layer elements and local refinement. Step 4: Physiological boundary conditions were prescribed. Step 5: Computational fluid-dynamics simulations were performed. Step 6: Simulation outputs were post-processed and analyzed.

2.2. Computational hemodynamics

In this study, the blood flow was assumed to be an incompressible non-Newtonian fluid. Given that the Reynolds number in the portal venous system remains below 1500, the flow was assumed to be laminar throughout the computational domain. The governing equations were three-dimensional incompressible Navier-Stokes equation and continuity equation.

Blood was modeled as an incompressible, non-Newtonian fluid, and laminar flow was assumed throughout. Flow was governed by the three-dimensional, incompressible Navier-Stokes and continuity equations [17]:

$$\rho \left(\frac{\partial \boldsymbol{u}}{\partial t} + \boldsymbol{u} \cdot \nabla \boldsymbol{u} \right) = -\nabla p + \nabla \cdot \boldsymbol{\tau} \tag{1}$$

$$\nabla \cdot \boldsymbol{u} = 0 \tag{2}$$

where \boldsymbol{u} is the velocity vector, ρ is the blood density (1050 kg/m³), p is pressure, and $\boldsymbol{\tau}$ is the viscous stress tensor.

The shear-dependent viscosity was characterized with the Carreau model [12],[31]:

$$\mu(\dot{\gamma}) = \mu_{\infty} + (\mu_0 - \mu_{\infty}) \left[1 + (\lambda \dot{\gamma})^2 \right]^{\frac{n-1}{2}}$$
(3)

with zero-shear viscosity μ_0 =0.056 kg/ms, infinite-shear viscosity μ_{∞} =0.00345 kg/ms, relaxation time λ = 3.31 s, and power-law index n = 0.36.

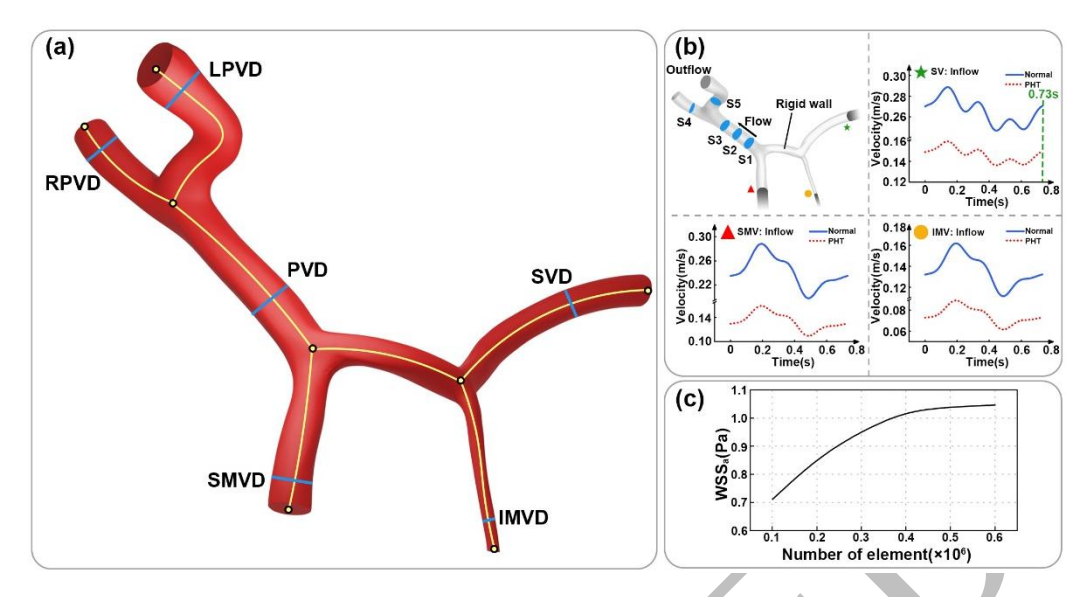


Figure 2 (a) Three-dimensional reconstruction of the portal-venous system. (b) Boundary conditions and Doppler-derived velocity waveforms at superior mesenteric vein (SMV), splenic vein (SV) and inferior mesenteric vein (IMV) and representative axial slices at five key locations. (c) Mesh-independence study showing convergence of average wall shear stress as the element count rises.

2.3. Boundary conditions

In routine clinical practice, patient-specific lobar venous pressures are rarely available in vivo, while Doppler inflows are obtainable and reliable for PV/SMV/SV/IMV. Figure 2(b) illustrates the resting-state velocity profiles prescribed at the inlets; for the PHT cohort, inlet flow rates were set to 0.5517 of the healthy values; this value is developed through previous work [24]. Outflow conditions were imposed at the right and left portal branches (RPV and LPV) (0.6 for the RPV and 0.4 for the LPV) [8]. Vessel walls were assumed rigid with a no-slip condition.

2.4. Calculation process

All models were discretized in ANSYS ICEM CFD (ANSYS, Canonsburg, PA). Because of the complex vessel anatomy, an unstructured grid was selected for its flexibility and robustness. A prismatic boundary layer consisting of 5 inflation layers was applied to every wall; the first-layer height was 0.01 mm and grew geometrically toward the core. Grid convergence was evaluated by tracking the time-averaged wall-shear stress (WSS_a) for meshes ranging from 0.1 to 0.8 million

Differences became negligible beyond roughly 0.5 million elements, a resolution adopted for all subsequent simulations to balance accuracy and computational cost. Flow simulations were performed in Fluent (ANSYS, Canonsburg, PA, USA). A transient simulation was performed with a timestep of 0.00292 s, corresponding to 1000 timesteps per cardiac cycle (0.73 s). A total of four cardiac cycles (2.92 s) were simulated to achieve periodic stability, and convergence was accepted when residuals fell below 1×10^{-5} . Pressure–velocity coupling employed the SIMPLE scheme with second-order upwind discretization to preserve numerical accuracy. All hemodynamic quantities reported were taken from the third simulated cardiac cycle.

2.5. Hemodynamic analysis

The hemodynamic parameters—TAWSS, OSI, and RRT—are key indicators for evaluating local blood flow characteristics and endothelial shear environment. These parameters were quantitatively derived from WSS, and were calculated using the following equations.

$$TAWSS = \frac{1}{T} \int_0^T |\mathbf{WSS}(s,t)| \cdot dt$$
 (4)

$$OSI = \frac{1}{2} \left[1 - \left(\frac{\left| \int_{0}^{T} \mathbf{WSS}(s,t) \cdot dt \right|}{\int_{0}^{T} \left| \mathbf{WSS}(s,t) \right| \cdot dt} \right) \right]$$
 (5)

$$RRT = \frac{1}{(1 - 2 \cdot OSI) \cdot TAWSS} \tag{6}$$

Here, T is the cardiac cycle duration, s denotes a point on the vessel wall, and t is time.

Hemodynamic risk thresholds were defined relative to the healthy control model, given the lack of portal-specific reference values in the literature. Regions with TAWSS below 50% of the healthy model's mean value were considered low-shear zones. Areas where the OSI or RRT exceeded 1.5 times than their corresponding healthy means were classified as adverse hemodynamic regions. This relative definition allowed us to systematically compare the distribution of risk-prone areas between the normal and PHT models. Disturbed shear regions were defined by TAWSS ≤ 0.523 Pa, OSI ≥ 0.0145 , RRT ≥ 2.548 Pa⁻¹.

To visualize the helical flow patterns within the venous system, this study introduces the dimensionless parameter Local Normalized Helicity (LNH) [2].

$$LNH = \frac{\mathbf{v} \cdot \boldsymbol{\omega}}{|\mathbf{v}| \cdot |\boldsymbol{\omega}|} = \cos \gamma \tag{7}$$

where v denotes the velocity vector, ω represents the vorticity vector, and γ is the angle between them. An LNH value of 1 indicates perfect alignment (same direction and orientation), whereas -1 indicates complete anti-alignment (same direction, opposite orientation). The sign of LNH also distinguishes the handedness of the helical flow, with positive and negative values corresponding to right-handed and left-handed helicity, respectively.

3 Results

3.1 Flow pattern

As illustrated in Figure 3, distinct differences in velocity distribution patterns were observed between the normal and PHT groups. Figure 3(a) clearly demonstrates that the overall blood flow velocity in the normal model was consistently higher than that in the PHT model, with the most pronounced discrepancy located at the confluence of SMV and the SV. Notably, both models exhibited helical flow patterns in the PV main trunk following venous confluence; however, the normal model presented more coherent and intensified helical structures. These differences were evident at both the peak systolic phase (T₁) and end-systolic phase (T₂), suggesting that PHT alters the dynamic nature of helical flow throughout the cardiac cycle.

Figure 3(c) further provides cross-sectional comparisons of axial velocity contours at five representative planes: S₁, S₂, and S₃ along the main trunk of the PV, and S₄ and S₅ at the right and left portal veins, respectively. In the normal model, cross-sections S₁ to S₃ at T1 displayed larger high-velocity regions compared to T₂, indicating strong pulsatile flow behavior. Conversely, the velocity distribution at S₅ showed minimal variation between T₁ and T₂, suggesting relatively stable flow in the left portal branch. In contrast, the PHT model exhibited more uniform and dampened velocity distributions across all sections, with less temporal fluctuation between T₁ and T₂. Additionally, the S₅ plane in the PHT model demonstrated a larger proportion of low-velocity regions compared to the normal model, potentially reflecting impaired hepatic perfusion.

An important observation is that in the normal model, cross-sections S1, S2, and S3 displayed two

prominent high-velocity zones originating from the SMV and SV inflows, respectively. These converging flows contributed to the formation of distinct rotational structures within the main PV. Although a similar dual-inflow pattern was identified in the PHT model, the associated high-velocity zones were less defined and spatially dispersed, implying a loss of flow coherence and kinetic energy due to elevated resistance and altered hemodynamic conditions. These findings suggest that portal hypertension not only reduces overall flow velocity but also attenuates the spatial heterogeneity and dynamism of venous blood flow.

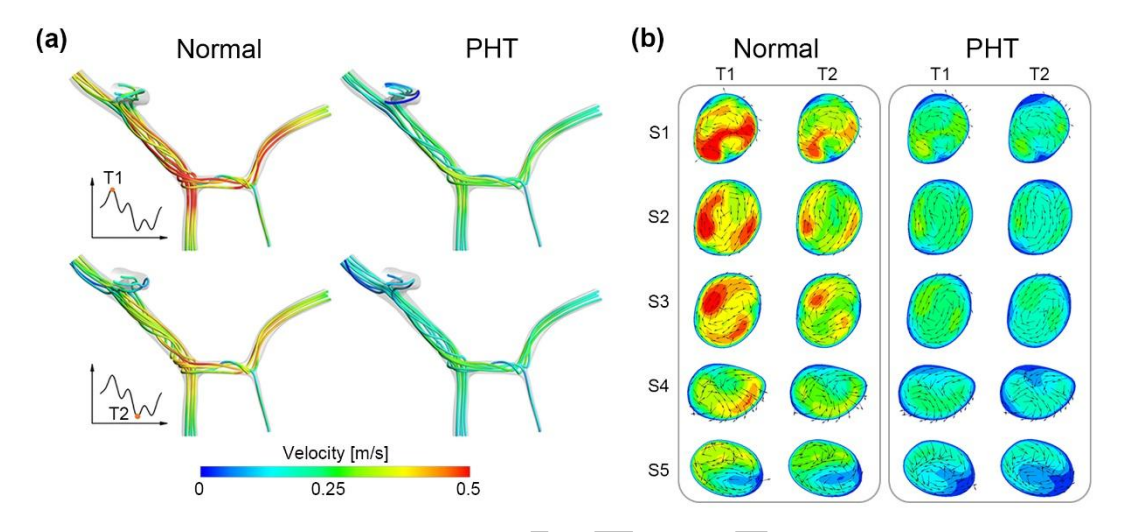


Figure 3 (a) Streamline visualization of the portal-venous system in the normal and PHT models. (b) Axial-velocity contours and in-plane velocity vectors at cross-sections S1-S5 for both models.

3.2 TAWSS, OSI and RRT

Figure 4 illustrates the spatial distribution of three key hemodynamic indicators in both the normal and PHT models. As shown in Figure 4(a) and (b), the TAWSS in the normal model was consistently higher than that in the PHT model, whereas the RRT was markedly lower. The distribution of OSI exhibited comparable patterns between the two models, though with some local variations. Further examination of the adverse hemodynamic zones—defined as regions with TAWSS ≤ 0.523Pa, OSI ≥ 0.0145, RRT ≥ 2.548Pa⁻¹—is presented in Figure 4(c). In both models, these risk zones were consistently located at hemodynamically vulnerable sites, including the bifurcation of the left and right portal veins, and the confluence region of the SMV and SV. These geometric features are prone to complex flow disturbances, and the observed clustering of low TAWSS and high RRT in these areas reinforces their susceptibility to pathological remodeling.

Quantitative comparisons are summarized in Figure 4(d). In the PHT model, the total surface area exposed to low TAWSS was nearly three times that of the normal model, while the area with high RRT values was approximately twice as large. Interestingly, the normal model exhibited slightly greater high OSI regions compared to the PHT model. This may reflect the fact that under physiologic flow conditions, greater shear oscillations occur near bifurcations due to stronger pulsatile effects and more dynamic flow redistribution, whereas the dampened and homogenized flow in the PHT model leads to reduced OSI despite pathological remodeling.

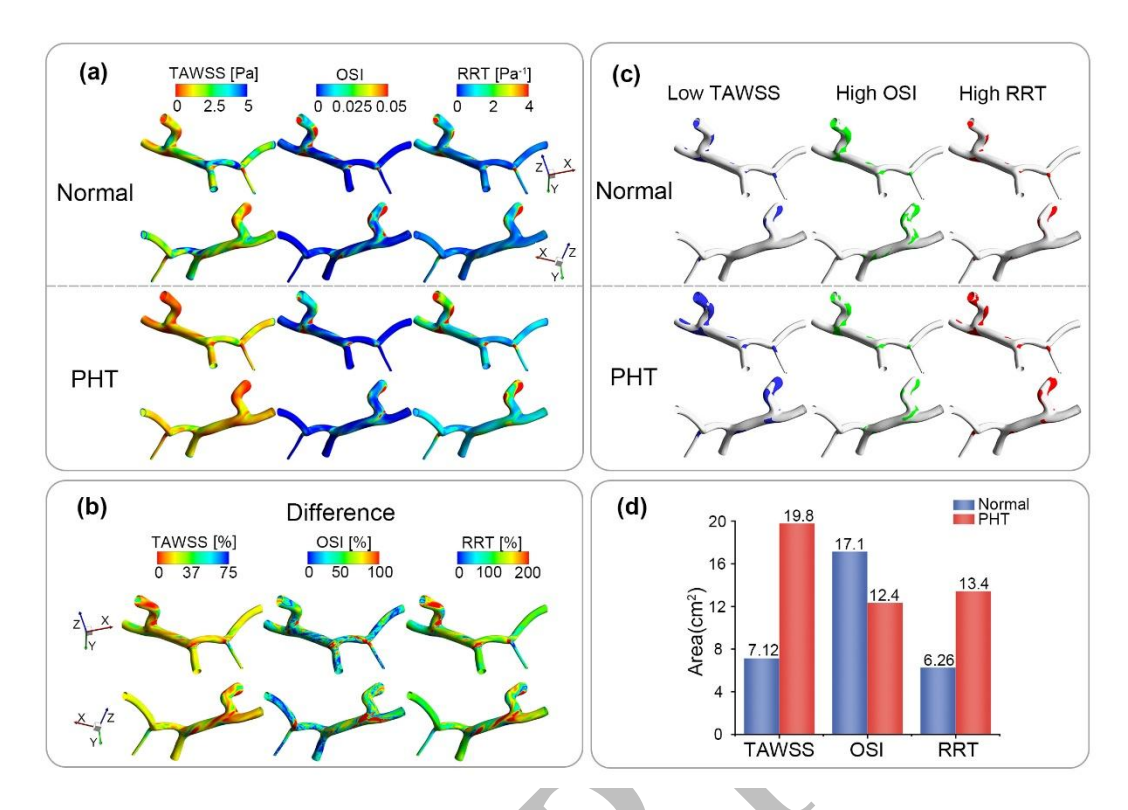


Figure 4 (a) Distribution clouds of TAWSS, OSI and RRT for the normal and PHT geometries. (b) Quantitative comparison of mean TAWSS, OSI and RRT between the two models. (c) Regions exhibiting adverse hemodynamics (TAWSS \leq 0.523Pa, OSI \geq 0.0145, RRT \geq 2.548Pa⁻¹). (d) Corresponding surface areas of these disturbed-flow zones.

3.3 Helical Flow

Figure 5 provides a comparative analysis of helical flow patterns between the normal and PHT models, focusing on both qualitative and quantitative aspects of left- and right-handed helicity. As shown in Figure 5(a), three-dimensional isosurface visualizations reveal distinct differences in helical flow strength and distribution. In the normal model, well-organized and prominent helical flow structures were observed throughout the portal venous trunk, with a clear presence of both right-handed (red) and lefthanded (blue) vortices. In contrast, the PHT model exhibited attenuated and disorganized helical flow, particularly in the proximal segments of the main portal vein, indicating a disruption in the natural rotational motion of blood induced by elevated portal pressure. These observations are quantitatively corroborated in Figure 5(b), which compares the cross-sectional distribution of left- and right-handed helical flow at three key locations along the main portal vein (S₁-S₃). In all sections, the normal model demonstrated a greater total area of helical flow, underscoring its preserved rotational dynamics. Moreover, the proportion of right-handed versus left-handed flow differed notably between the two models. Figure 5(c-d) further quantifies these trends by calculating the ratio of left- to right-handed helicity along the main portal venous axis. Both models exhibited a progressive increase in left-handed helicity from the confluence of the SMV and SV toward the bifurcation of the portal vein. However, this shift was markedly more pronounced in the PHT model. At the S₃ location, for example, the left-to-right helical flow ratio reached approximately 3:1 in the PHT model, compared to a more balanced distribution in the normal model.

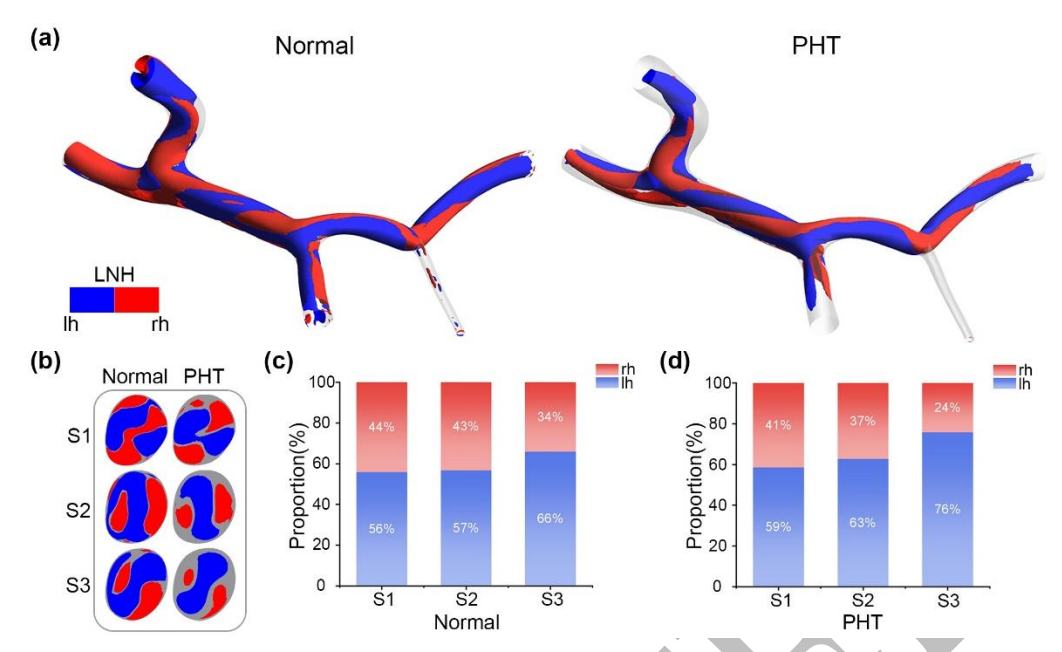


Figure 5 (a) Cycle-averaged isosurfaces of local normalized helicity (LNH) illustrating left-handed (LNH < -0.9) and right-handed (LNH > 0.9) helical structures in both models. (b) LNH distributions on slices S1–S3, where the largest inter-model differences occur. Left-handed (LNH<-0.9) and right-handed (LNH>0.9) helical structures are represented in blue and red, respectively, with gray indicating between the two. (c, d) Percentage of left-handed and right-handed helicity in the normal versus PHT models.

4 Discussion

Portal hypertension represents a pivotal pathophysiological milestone in the progression of cirrhosis and is the immediate driver of life-threatening sequelae such as variceal hemorrhage and portal-vein thrombosis. With the advent of patient-specific CFD, it has become feasible to interrogate portal hemodynamics at a level of spatial and temporal resolution unattainable by conventional imaging alone, thereby providing mechanistic insight and refined risk stratification. In the present investigation, we reconstructed subject-specific three-dimensional portal-venous geometries and compared hemodynamic metrics—velocity magnitude, TAWSS, RRT and local normalized helicity—between healthy controls and individuals with portal hypertension throughout an entire cardiac cycle. These quantitative comparisons furnish a biomechanical framework that links altered flow dynamics to the spectrum of PHT-related complications.

Hemodynamic analysis revealed that portal-hypertensive geometry fundamentally alters flow delivery and near-wall mechanics. Mean axial velocity in the main portal trunk decreased by ~45 % relative to the healthy model, reflecting both elevated downstream resistance and the steal phenomenon created by collateral pathways. This global deceleration was accompanied by pronounced local disturbances at the SMV-SV confluence and at the origin of the right and left portal branches. In these regions, TAWSS frequently fell below the physiological threshold of 0.523 Pa, whereas OSI exceeded 0.0145 and RRT rose above 2.548 Pa⁻¹—values previously linked to endothelial dysfunction, inflammatory gene upregulation and platelet adhesion. Such a "low-shear/high-oscillation" micro-environment is concordant with idealized-model findings and provides a plausible mechanical substrate for the high prevalence of portal-vein thrombosis observed clinically in PHT.

Beyond thrombogenic risk, shear redistribution also affects lobar perfusion. In the hypertensive model we observed a left-ward bias of splenic-vein inflow, consistent with the CFD results of Liang et al., who

demonstrated that geometrical distortion preferentially channels hepatotropic SV blood towards the left lobe. Concomitantly, reduced flow and diminished WSS in the right branch may impair nutrient and oxygen delivery, offering a mechanistic explanation for the right-lobe atrophy/left-lobe hypertrophy pattern frequently reported in advanced cirrhosis. These findings underscore that the hemodynamic consequences of portal hypertension are not confined to pressure elevation alone but encompass profound spatial remodeling of shear stress, residence time and flow partitioning — factors that synergistically drive thrombotic events and structural liver changes.

Our findings align with and extend previous computational and experimental investigations into portal venous hemodynamics. The observed reduction in mean flow velocity and WSS in the PHT model is consistent with Doppler ultrasound measurements reported by Sherbiny et al. [7],[30]. Similarly, some works [22],[23] used CFD modeling to demonstrate that thrombosis and vascular obstruction markedly alter local shear distribution and secondary flow structures, which agrees with the disrupted WSS and elevated RRT observed in our simulations. Moreover, the link between low WSS and prothrombotic endothelial activation observed in our model echoes the mechanobiological mechanisms proposed by Yao et al. [28] and Wang et al. [23], where abnormal shear stress was shown to trigger inflammatory signaling and coagulation factor upregulation. Collectively, these comparisons indicate that our findings are not isolated but rather build upon and complement the established understanding of portal hemodynamics, while also extending it by highlighting helicity as a potentially important yet previously overlooked feature in PHT pathophysiology.

An important observation from our CFD analysis is the presence of helical flow structures in both the normal and PHT portal venous models, particularly along the main portal vein and its bifurcation. Although the overall magnitude of helicity showed no significant difference between the two groups, noticeable variations were observed in its spatial distribution and structural organization. In the normal model, a more stable, continuous, and bilaterally symmetric helical flow pattern was present at the confluence of the SMV and SV, whereas in the PHT model, this structure appeared weakened and spatially heterogeneous. This indicates strong alignment between rotational and axial flow components, which contributes to sustained and uniform wall shear stress. In contrast, the PHT model demonstrated a marked attenuation of helical structures at the same locations. The distribution of left- and right-handed helicity became asymmetric. These changes were accompanied by an expansion of near-wall regions characterized by low WSS and elevated RRT. Helical flow has been recognized as a protective biomechanical mechanism in vascular systems, promoting "selfcleaning" effects that limit flow stagnation, suppress platelet adhesion, and preserve the antiinflammatory phenotype of endothelial cells [6],[20]. Therefore, the diminished helicity observed in PHT conditions may reflect a loss of these protective effects, potentially facilitating thrombus formation (PVT) and variceal proliferation. Notably, in the PHT model, localized peaks in helicity were observed near the proximal branches of the left and right portal veins, closely aligning with regions of steep WSS gradients. This suggests a compensatory restructuring of flow in response to geometric deformation. While such localized increases in LNH may transiently support shear force homeostasis, their spatial heterogeneity could exacerbate endothelial stress, contributing to maladaptive remodeling processes.

Taken together with TAWSS, OSI, and RRT distributions, these findings support the hypothesis that disruption and redistribution of helical flow are mechanistic contributors to early endothelial dysfunction and subsequent thrombotic events in PHT. This study highlights helicity—particularly LNH—as a promising metric for evaluating flow quality and stratifying thrombotic risk in patients

with portal hypertension. Future investigations integrating large-cohort imaging and 4D-flow MRI could further elucidate the clinical significance of helical flow impairment. Moreover, endovascular strategies aimed at restoring favorable helical patterns—such as catheter-based modulation or flow-directing devices—may offer novel therapeutic avenues for mechanical intervention in PHT. Beyond these hemodynamic parameters, sustained high portal pressure may also induce progressive alterations in the vascular wall itself. Chronic exposure to abnormal shear stress gradients and elevated transmural pressure can promote endothelial dysfunction, smooth muscle proliferation, and extracellular matrix deposition, thereby contributing to vascular stiffening and luminal narrowing. In parallel, the adaptive remodeling of the venous wall may further distort local geometry, exacerbating recirculation zones and reducing flow efficiency. These mechanical and structural changes, in turn, reinforce the pathophysiological cycle of elevated resistance and impaired perfusion within the portal system. Collectively, the interaction between abnormal flow dynamics and vascular wall remodeling underlies the transition from compensated portal hypertension to its decompensated stage, highlighting the importance of integrated biomechanical analysis for understanding disease progression.

While this study provides new insights into the hemodynamic alterations and helicity disruption associated with PHT, several limitations should be acknowledged. First, the boundary conditions adopted in our simulations primarily relied on Doppler-derived inflow waveforms combined with traction-free outlet settings, a widely accepted approach when patient-specific portal and lobar venous pressure data are unavailable in vivo. This strategy allowed us to focus on relative changes in near-wall shear metrics (WSS, OSI, RRT, helicity), which are closely linked to endothelial function and thrombosis, but it does not fully reproduce the absolute pressure conditions characteristic of PHT. Consequently, the simulated pressure field may deviate from physiological values, potentially influencing local flow dynamics and pressure–flow interactions. Future work will incorporate pressure-controlled or resistance-type outlet models calibrated to clinically measured portal pressures to enhance physiological accuracy and enable direct analysis of pressure effects. Despite the limitation, the key findings—such as reduced flow velocity, expanded low-shear and high-residence regions, and marked attenuation of helical flow near bifurcations—were robust across model variations, highlighting the importance of flow structure and helicity loss as mechanistic contributors to thrombosis and vascular remodeling in portal hypertension.

5. Conclusion

In this study, the patient-specific the portal-venous model and CFD simulations were employed to systematically investigate the hemodynamic alterations associated with PHT. Compared to the healthy condition, the PHT model exhibited reduced flow velocity, expanded regions of low WSS, and elevated RRT, particularly at bifurcation sites—indicating a pro-thrombotic microenvironment. Moreover, helical flow, a structure known for its protective effects on vascular function, was markedly weakened in the PHT model, especially near the main portal vein bifurcation, where pathological changes often initiate. These findings suggest that disruption of physiological helicity may play a critical role in endothelial dysfunction, thrombus formation, and liver lobe remodeling. Overall, this study underscores the potential of helicity-based metrics as biomechanical indicators for assessing thrombotic risk and guiding future therapeutic strategies in portal hypertension.

Acknowledgements

This work is supported by National Natural Science Research Foundation of China (No. 12372305, 12272153, 12202274, 11902126), Changzhou Science and Technology Support Program (Changzhou

Science and Technology Support Program (CJ20241077), the Clinical Research Project of Changzhou Medical Center of Nanjing Medical University (CMCC202304) and Outstanding young backbone teacher of Jiangsu Qinglan Project, Postgraduate Research & Practice Innovation Program of Jiangsu University of Technology (XSJCX24_66), Zhongwu young innovative talents projection from Jiangsu Institute of Technology.

Declaration of Conflicting Interests

All authors declare no competing interests.

Ethics Statement

The study was conducted in accordance with the Declaration of Helsinki and was approved by the Ethics Committee of the Second People's Hospital of Changzhou (No. 2022KY120-01). All participants in the study were provided with comprehensive information about the study and provided their informed consent by signing the appropriate documentation.

Authors contribution

Zhenmin Fan and Haonan Li conceived the idea; Zhenmin Fan, Haonan Li and Xiaoyan Deng conducted the analyses; Zhenmin Fan, Haonan Li, and Zhixiang Zhang provided the data; Zhenmin Fan and Haonan Li wrote the paper; all authors contributed to the writing and revisions.

Reference

- [1] Augustin H.G.Koh G.Y., Organotypic vasculature: From descriptive heterogeneity to functional pathophysiology, Science, 2017.
- [2] Calo K., Capellini K., De Nisco G., Mazzi V., Gasparotti E., Gallo D. et al., Impact of wall displacements on the large-scale flow coherence in ascending aorta, J Biomech, 2023, 111620.
- [3] Davignon J.Ganz P., Role of endothelial dysfunction in atherosclerosis, Circulation, 2004, III27-32
- [4] De Franchis R.Baveno V.I.F., Expanding consensus in portal hypertension: Report of the Baveno VI Consensus Workshop: Stratifying risk and individualizing care for portal hypertension, J Hepatol, 2015, 743-52.
- [5] De Franchis R.,Bosch J.,Garcia-Tsao G.,Reiberger T.,Ripoll C.Baveno V.I.I.F., Baveno VII Renewing consensus in portal hypertension, J Hepatol, 2022, 959-974.
- [6] De Nisco G., Hoogendoorn A., Chiastra C., Gallo D., Kok A.M., Morbiducci U.Wentzel J.J., The impact of helical flow on coronary atherosclerotic plaque development, Atherosclerosis, 2020, 39-46.
- [7] El Sherbiny W., Abdelrahman A., Diasty M. Shaltout S.W., Changes in Doppler parameters of portal pressure after interventional management of hepatocellular carcinoma, Abdom Radiol (NY), 2016, 1532-8.
- [8] George S.M., *Hemodynamic investigation of the liver using magnetic resonance imaging and computational fluid dynamics*, Georgia Institute of Technology2008.
- [9] Hyodo R., Takehara Y., Mizuno T., Ichikawa K., Horiguchi R., Kawakatsu S. et al., Four-dimensional Flow MRI Assessment of Portal Hemodynamics and Hepatic Regeneration after Portal Vein Embolization, Radiology, 2023, e230709.
- [10] Li D., Wang J., Zeng W., Zeng X., Liu Z., Cao H. et al., The loss of helical flow in the thoracic aorta might be an identifying marker for the risk of acute type B aortic dissection, Comput Methods Programs Biomed, 2023, 107331.
- [11] Li X., Wang X.K., Chen B., Pu Y.S., Li Z.F., Nie P.Su K., Computational hemodynamics of portal vein hypertension in hepatic cirrhosis patients, Biomed Mater Eng., 2015, S233-43.

- [12] Lu J.,Fan Z.,Ye X.,Deng X.,Feng H.Liu M., Impact of lower limb movements on iliac vein stenting in iliac vein compression syndrome patients: insights from computational modeling, Acta Bioeng Biomech, 2024, 23-35.
- [13] Mooradian D.L., Hutsell T.C. Keefer L.K., Nitric oxide (NO) donor molecules: effect of NO release rate on vascular smooth muscle cell proliferation in vitro, J Cardiovasc Pharmacol, 1995, 674-8.
- [14] Petkova S., Hossain A., Naser J. Palombo E., *CFD modelling of blood flow in portal vein hypertension with and without thrombosis*, Third international conference on cfd in the minerals and process industries csiro, melborne, australia, 2003, pp. 10-12.
- [15] Pinzani M.,Rosselli M.Zuckermann M., Liver cirrhosis, Best Pract Res Clin Gastroenterol, 2011, 281-90
- [16] Prakash S.,Bies J.,Hassan M.,Mares A.Didia S.C., Portal vein thrombosis in cirrhosis: A literature review, Front Med (Lausanne), 2023, 1134801.
- [17] Qian S.,Ma T.,Zhang N.,Liu X.,Zhao P.,Li X. et al., Spatiotemporal transfer of nitric oxide in patient-specific atherosclerotic carotid artery bifurcations with MRI and computational fluid dynamics modeling, Comput Biol Med, 2020, 104015.
- [18] Qiu Y.,Tai Y.,Lei J.,Zeng Y.,Wu H.Li K., Modelling the liver region as porous media to noninvasively measure portal vein pressure gradient (PPG) with numerical methods, J Biomech, 2023, 111660.
- [19] Ripoll C., Groszmann R., Garcia-Tsao G., Grace N., Burroughs A., Planas R. et al., Hepatic venous pressure gradient predicts clinical decompensation in patients with compensated cirrhosis, Gastroenterology, 2007, 481-8.
- [20] Stonebridge P.A., Vermassen F., Dick J., Belch J.J. Houston G., Spiral laminar flow prosthetic bypass graft: medium-term results from a first-in-man structured registry study, Ann Vasc Surg, 2012, 1093-9.
- [21] Van Steenkiste C., Trachet B., Casteleyn C., Van Loo D., Van Hoorebeke L., Segers P. et al., Vascular corrosion casting: analyzing wall shear stress in the portal vein and vascular abnormalities in portal hypertensive and cirrhotic rodents, Lab Invest, 2010, 1558-72.
- [22] Wang T.,Yong Y.,Ge X.Wang J., A computational model-based study on the feasibility of predicting post-splenectomy thrombosis using hemodynamic metrics, Front Bioeng Biotechnol, 2023, 1276999.
- [23] Wang T., Zhou Z.Liang F., Influences of Anatomorphological Features of the Portal Venous System on Postsplenectomy Hemodynamic Characteristics in Patients With Portal Hypertension: A Computational Model-Based Study, Front Physiol, 2021, 661030.
- [24] Wei W., Pu Y.S., Wang X.K., Jiang A., Zhou R., Li Y. et al., Wall shear stress in portal vein of cirrhotic patients with portal hypertension, World J Gastroenterol, 2017, 3279-3286.
- [25] Wild N.C., Bulusu K.V. Plesniak M.W., Vortical Structures Promote Atheroprotective Wall Shear Stress Distributions in a Carotid Artery Bifurcation Model, Bioengineering (Basel), 2023.
- [26] Wu X.,Xiao H.Ma L., The application of computational fluid dynamics in hepatic portal vein haemodynamics research: a narrative review, Quant Imaging Med Surg, 2025, 2605-2620.
- [27] Yan Y.,Xiong Z.,Wang X.,Yang L.,Zheng T.Luo X., A novel potential mechanism for the development of portal vein thrombosis in cirrhosis based on portal hemodynamics, Insights Imaging, 2022, 192.
- [28] Yao H.Wang Y., Relationship between hemodynamic parameters and portal venous pressure in cirrhosis patients with portal hypertension, Open Life Sci, 2020, 981-987.

[29] Zarins C.K., Giddens D.P., Bharadvaj B.K., Sottiurai V.S., Mabon R.F. Glagov S., Carotid bifurcation atherosclerosis. Quantitative correlation of plaque localization with flow velocity profiles and wall shear stress, Circ Res, 1983, 502-14.

[30] Zhang L., Duan Y.Y., Li J.M.Yin J.K., Hemodynamic features of Doppler ultrasonography in patients with portal hypertension: intraoperative direct measurement of portal pressure in the portal venous system, J Ultrasound Med, 2007, 1689-96.

[31] Zhang X.,Fan Z.,Liu X.,Liu M.,Ye X.Deng X., Hemodynamic impact of snoring on carotid artery after stent implantation: the role of oscillation, Acta Bioeng Biomech, 2023, 35-45.

